Hexagonal Superalignment of Nano-Objects with Tunable Separation in a Dilute and Spacer-Free Solution

Chien-You Su,[1,*] Qiang Lyu,[2,*] Dun-Yen Kang,[3,*,†] Zhi-Huei Yang,[3] Chon Hei Lam,[3] Yu-Hsiang Chen,[4] Shen-Chuan Lo,[4] Chi-Chung Hua,[1,‡] and Li-Chiang Lin[2,§]

[1]*Department of Chemical Engineering, National Chung Cheng University, No.168, Sec. 1, University Rd., Minhsiung, Chiayi 62102, Taiwan*

[2]*William G. Lowrie Department of Chemical and Biomolecular Engineering, The Ohio State University, 151 W. Woodruff Ave., Columbus, Ohio 43210, USA*

[3]*Department of Chemical Engineering, National Taiwan University, No. 1, Sec. 4, Roosevelt Road, Taipei 10617, Taiwan*

[4]*Dept. Electron Microscopy Development and Application, Materials and Chemical Research Laboratories, Industrial Technology Research Institute, No. 195, Chung Hsing Road, Sec. 4, Hsinchu 31040, Taiwan*

(Received 31 July 2019; published 6 December 2019)

Manipulating building-block nanomaterials to form an ordered superstructure in a dilute and spacer-free solution phase challenges the existing 5-nm node lithography and nanorobotics. The cooperative nature of nanocrystals, polymers, and cells can lead to superarrays or colloidal crystals. For known highly ordered systems, the characteristic length of materials, defined as the shortest dimension of objects, is generally larger than their separations. A spacer (small-molecule surfactant or polymer) is typically required to diminish short range van der Waals attraction, which results in a glassy or liquid state. Herein we propose a new concept of achieving highly ordered nano-objects in a dilute and spacer-free system *via* the synergistic effects of excellent solvation and appropriate constraints on rotational motion. As a proof of concept, this study demonstrates that aluminosilicate nanotubes (AlSiNTs) suspended in water under dilute conditions (e.g., 1.0 wt%) can spontaneously form hexagonal arrays with an intertubular distance as large as tens of nanometers. The separation distance of the ordered superstructure is also tunable via controlling the concentration and length of nanotubes. These superaligned structures are probed using small-angle x-ray scattering and cryo-TEM characterizations, with underlying mechanisms investigated at an atomic level using molecular dynamics simulations. The concept and discovery of this work can open up opportunities to a variety of applications including visible-UV photonics and nanolithography, and may be generalizable to other nano-object systems that fulfill similar requirements.

DOI: 10.1103/PhysRevLett.123.238002

Introduction.—Tremendous effort has been made for the controlled self-assembly of inorganic nanomaterials [1–4], macromolecules [5–7], and biomolecules [8–11] to form highly ordered superstructures or colloidal crystals either at the interface or in the bulk liquid phase. For example, it has been reported that ordered superlattices of hexagonal nanoplates form at the liquid-air interface of a hexane wetting layer [1]. The characteristic length of these ordered nano-objects is approximately 20 nm while the interparticle separation, controlled by oleic acid, is below 10 nm. Gold nanoparticles, decorated by nitrilotriacetic acid and segregated by proteasome protein, also form ordered arrays in the solution phase [11]. In general, colloidal particles of a dimension of 10^1 to 10^4 nm with sufficient long-range repulsion have been identified to form an ordered colloidal crystal phase, if the volume fraction of the particles, whose external surface may be decorated, goes beyond a critical value (e.g., 68 vol% for a body-centered cubic) [12]. In these systems, spacers (e.g., surfactants, acids, or polymers) play a critical role in preventing noncooperative coagulation, suppressing the Brownian motion, and organizing nano-objects to form ordered superstructures, wherein the dimension of the spacers determines the separation between adjacent nano-objects.

Achieving highly ordered superstructures or colloidal crystals in the dilute solution phase (objects with a long-distance separation) in the absence of spacer molecules remains a great challenge. To introduce the repulsive interactions or to weaken the attraction between nanoparticles, good solvation or addition of surfactants is commonly needed. Under those conditions the predominant Brownian diffusion results in dispersed colloidal solution but impedes the alignment of the nanoparticles. We hypothesize that preserving the interparticle repulsion while also suppressing the Brownian motion of particles is the key to achieve ordered colloidal crystals in dilute and spacer-free solutions. Specifically, the interparticle repulsive forces can be created through good solvation, and the Brownian motion can be suppressed in colloidal systems of low-dimensional objects by constraining their rotational

 © 2019 American Physical Society

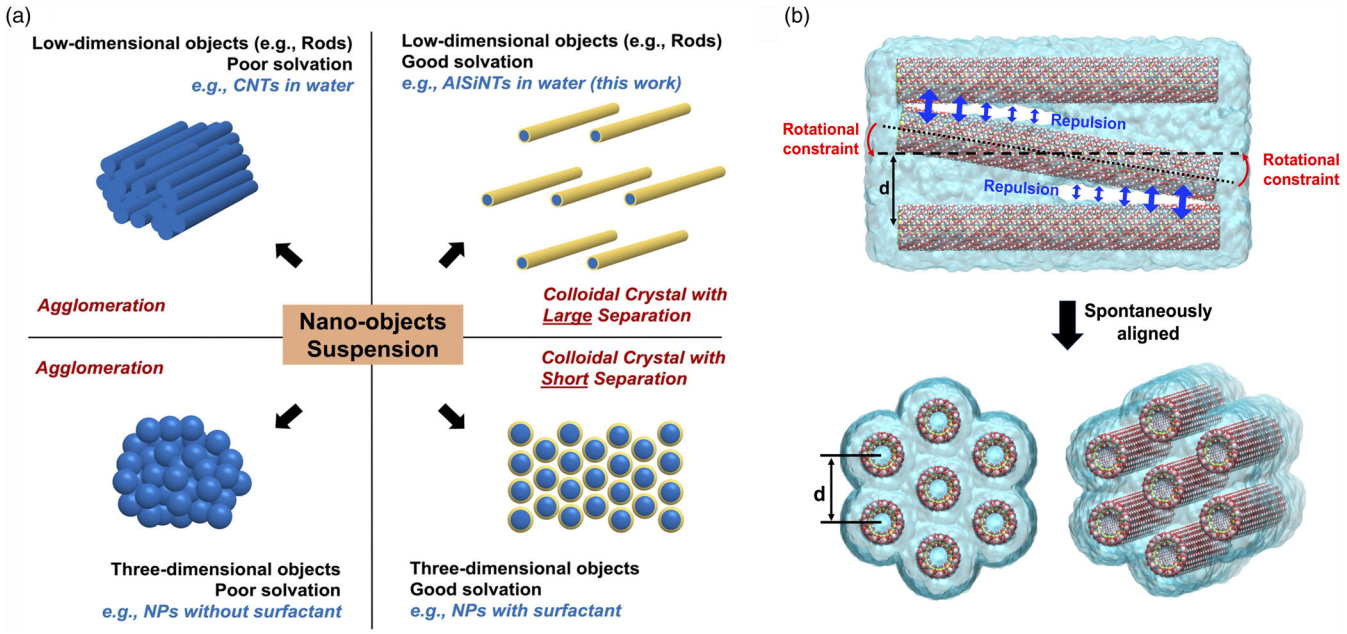

FIG. 1. (a) Schematic summary of solution phases for nano-object suspension. Different phases can be possibly formed in terms of the solvation degree and the dimensionality of the objects. Yellow represents good solvation of the objects. (b) Schematic of the spontaneously ordered one-dimensional objects via synergistic solvation effects and rotational constraints. For nanotubes with excellent solvation, the loss of solvation shell when proximate tubes get too close can introduce intertubular repulsive forces. This is anticipated to intrinsically constrain the rotational motion of the nanotubes and subsequently lead to an ordered colloidal phase.

motion. On the other hand, for systems without good solvation and/or comprising of three-dimensional objects, large-distance superalignment cannot be formed without a spacer or an external force. Davidson and co-workers recently observed a liquid-crystalline columnar phase of imogolite nanotubes under a notably more dilute condition as compared to other known columnar liquid crystals [13], which qualitatively supports our proposed hypothesis. A schematic summary of the hypothesis can be seen in Fig. 1(a). We also hypothesize that the concentration of nano-objects and their aspect ratio, due to their influence on rotational constraints, can affect their separation distance and in turn control the interparticle distance.

To test these hypotheses, systems comprising only highly hydrophilic aluminosilicate nanotubes (AlSiNTs, also known as synthetic imogolite) and water, systems in the absence of any spacers and external forces, are created. Excellent solvation should prevent proximate nanotubes from getting too close owing to the loss of solvation shell, thus providing the needed intertubular repulsion. As illustrated in Fig. 1(b), we anticipate that such intertubular repulsion, coupled with the high-aspect ratio of the nanotubes, can intrinsically constrain their rotational motion and therefore suppress the Brownian motion. In a dilute 1.0 wt% AlSiNT aqueous solution with a tube diameter of approximately 2 nm, a solution-phase hexagonal superalignment of AlSiNTs indeed forms with an intertubular separation of ~20 nm. Such highly ordered arrays are observed and quantitatively analyzed using bulk [small-angle x-ray scattering (SAXS)] and local [cryogenic transmission electron microscopy (cryo-TEM)] characterizations, with atomistic understandings from molecular dynamics (MD) simulations. Details regarding synthesis, SAXS, cryo-TEM, and computational approaches can be seen in methods of the Supplemental Material [14].

Ordered arrays with large separation probed by SAXS.—The SAXS characterizations reveal the formation of highly ordered AlSiNTs. Figure 2(a) (inset) shows the raw two-dimensional (2D) SAXS pattern of the 1.0 wt% dilute AlSiNT solution, and the sharp rings indicate the hexagonal arrangement. The scattering can also be well described by the product of the form factor for hollow cylinders [15] and the structure factor [16–18] describing the tube alignment with a hexagonal ordering (see methods in the Supplemental Material [14]). The tube radius and wall thickness of AlSiNT are determined from the form-factor analysis to be ~0.75 and ~0.3 nm, respectively, in agreement with a previous report [13]. The (un-normalized) structure factor shown in Fig. 2(b) can then be further extracted as the scattering intensity (Supplemental Material, Fig. S1a [14]) divided by the contribution of form factor. The four clear Bragg peaks with relative separations in the q space of $1:\sqrt{3}:\sqrt{4}:\sqrt{7}$ are again an unambiguous indication of a hexagonal positional order. The mean intertubular separation distance, $d(=4\pi/\sqrt{3}q_{100})$, is quantified to be ~23.3 nm for the 1.0 wt% AlSiNT solution. In this system, the tube length is estimated to be ~1.8 μm from the dynamic light scattering

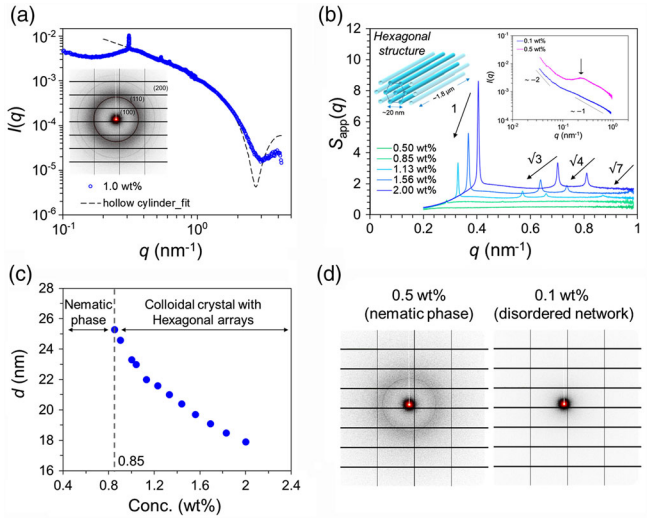

FIG. 2. Bulk characterizations using SAXS. (a) The scattering intensity of the 1.0 wt% AlSiNTs solution, and the inset displays the original 2D pattern with sharp rings that correspond to the hexagonal lattice peaks. (b) The un-normalized structure factors with various representative tube concentrations (0.5–2.0 wt%), and the inset shows the scattering intensities at two representative low concentrations that produce either a nematic phase (0.5 wt%) or disordered network (0.1 wt%). The complete dataset is given in the Supplemental Material, Fig. S1b [14]. (c) Intertubular separation as a function of tube concentration, with a sharp phase transition at a critical separation of ~25 nm. (d) Original 2D patterns for two representative low tube concentrations.

(DLS) analysis [19–21] (Supplemental Material, Fig. S2 [14]). Figure 2(c) and Supplemental Material Table S1 [14] show that the intertubular distance monotonically increases from ~18 to ~25 nm when the AlSiNT concentration reduces from 2.0 to 0.85 wt% without altering the alignment. This suggests that the intertubular separation can be controlled via the concentration. We also find that the position of the (100) peak demonstrates a power-law dependence on the concentration as $q_{100} \propto c^{0.4}$ (Supplemental Material, Fig. S1d [14]), with a scaling exponent close to 0.5 for the "2D swelling" law which has previously been assigned to the ordered structures formed by rigid rod [22] and tubular [23] molecules with high aspect ratios ($L/D \gg 1$). Meanwhile, the height for all four Bragg peaks [Fig. 2(b)] reduces with decreased concentrations and abruptly disappears below a concentration of 0.85 wt%, indicating a sharp transition from the hexagonal structure to the nematic one [13]. The intertubular distance at the critical concentration (0.85 wt%) is referred to as the critical separation distance (d^*). For AlSiNTs with a length of ~1.8 μm, the rotational constraint becomes insufficiently significant when the concentration goes below 0.85 wt%. As shown from the original 2D patterns in Figs. 2(a) and 2(d), the transition from a hexagonal phase (1.0 wt% AlSiNTs) to a nematic one (0.5 wt%) and, eventually, a disordered network (0.1 wt%) is observed. The corresponding scattering intensity profiles for the 0.5 and 0.1 wt% AlSiNT solutions can be seen in the inset of Fig. 2(b). The isotropic 2D pattern for the nematic phase [Fig. 2(d)] further indicates that, in addition to the impact of tube-length (and separation) distribution that would smear the originally anisotropic pattern, the average tube orientation of each local nematic microdomain likely points to a somewhat random direction in bulk solution. AlSiNTs with a length ~0.9 μm are also studied (Supplemental Material, Fig. S3 [14]). The short length weakens the rotational constraints. Consequently, the SAXS patterns present a broad peak, suggesting a nematic phase instead of hexagonal arrays (sharp patterns).

Cryo-TEM visualization.—Cryo-TEM is further employed as a quasiliquid state characterization, for the first time, to directly visualize the ordered phase of 1.8 μm AlSiNTs (Fig. 3). Consistent with SAXS, equally spaced AlSiNTs are observed in the 1.0 wt% [Fig. 3(a)] and 1.5 wt% solution [Fig. 3(b)]. The images of the 1.0 wt% solution show an intertubular separation of ~20 nm + / − ~1 nm, and 14.5 nm + / − ~1 nm for the 1.5 wt% solution. The small standard deviations (i.e., ~1 nm) evidently indicate the highly ordered array. The distance observed by cryo-TEM is shorter than that by SAXS, e.g., ~20 nm for the 1.5 wt% sample. The disagreement may come from the increased density of the vitreous ice (1.25 g cm^{-3}) [24]. The 0.1 wt%

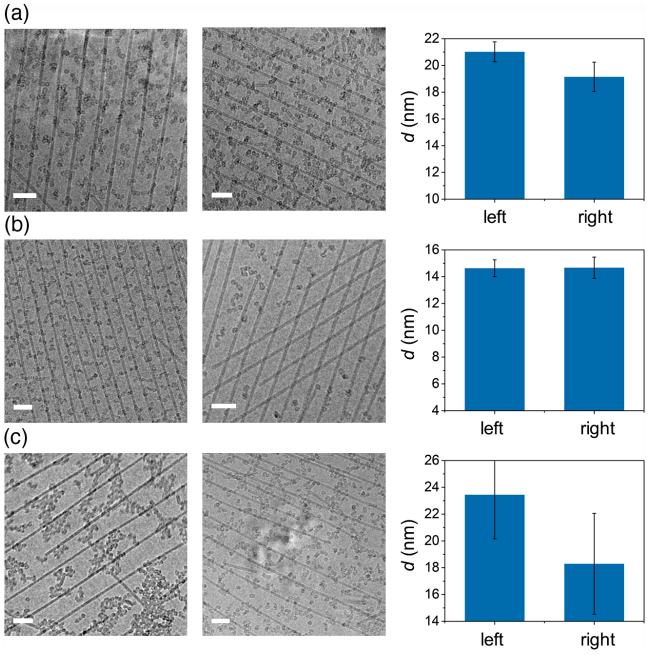

FIG. 3. Cryo-TEM visualizations. Images of (a) 1.0 and (b) 1.5 wt% AlSiNT solutions (tube length = ~1.8 μm), in which the AlSiNTs are nearly equally spaced. The average intertubular distances are summarized in the panels on the right. (c) Images and the average intertubular separations of the 1.0 wt % of AlSiNTs with an average length of ~0.9 μm, in which a relatively nonuniform separation is observed (i.e., larger error bars). The scale bar in each image is 20 nm. The circular objects displayed represent the precursor of AlSiNTs [25,26].

solution shows isotropic orientation in the cryo-TEM images (Supplemental Material, Fig. S4 [14]), which again agrees with SAXS. AlSiNTs with a shorter length of ~0.9 μm are also found to display a more disordered phase in terms of a more than 3 nm of standard deviation in their intertubular separation [Fig. 3(c)], suggesting a nematic phase instead of a colloidal crystal phase.

The Hermans orientation parameter (f_H) of the observed superarray is also computed, which is defined as the following:

$$f_H = \frac{3\langle \cos^2\phi \rangle - 1}{2}, \tag{1}$$

where

$$\langle \cos^2\phi \rangle = \frac{\sum_{\phi=0}^{\phi=\pi/2} N(\phi)\cos^2\phi \sin\phi}{\sum_{\phi=0}^{\phi=\pi/2} N(\phi)\sin\phi}. \tag{2}$$

In these equations, ϕ indicates the angle with respect to a reference axis, and $N(\phi)$ refers to the number of nanotubes. $f_H = 1$ represents a perfect alignment, whereas $f_H = 0$ indicates a randomly oriented distribution. f_H of the samples shown in Fig. 3 is found to be beyond 0.99. However, in some of the images [Fig. 3(b)], AlSiNT arrays present distinct orientations. This may be an artifact caused by the formation of the vitreous ice. The vitreous ice for imaging forms a thin disk with 5 to 500 nm in thickness [27,28], the same length scale as the intertubular separation. The out-of-plane alignment could be therefore strongly disturbed, resulting in two out-of-plane arrays stacking on the same focal plane (see Supplemental Material, Fig. S5 [14]). We note that the analysis of the intertubular separation as well as the orientation factor derived from the cryo-TEM images could be biased because TEM is regarded as local instead of bulk characterization and the formation of vitreous ice. Nonetheless, the cryo-TEM images presented herein serve as a visual support for the bulk quantitative analysis using SAXS.

MD simulations.—To achieve atomistic understandings, all-atom (AA) and coarse-grained (CG) MD simulations, using the LAMMPS package [29], are carried out. From the AA simulations of two parallel AlSiNTs suspended in water, Fig. 4(a) shows that a repulsive force indeed exists between proximate nanotubes in close proximity are less favorable than fully independent ones. This is caused by the solvation of the highly hydrophilic external surface of AlSiNTs (i.e., −OH groups). At a small intertubular distance (e.g., 3.2 Å), as shown in the inset of Fig. 4(a) and Supplemental Material Fig. S6 [14], a complete solvation shell surrounding the nanotubes cannot form and thus imposing a large AlSiNTs-water interaction penalty. As a comparison, proximate hydrophobic carbon nanotubes (CNTs) in water instead feature an attractive potential well [Fig. 4(a)]. Details of these AA calculations [30–33] can be found in the Supplemental Material [14].

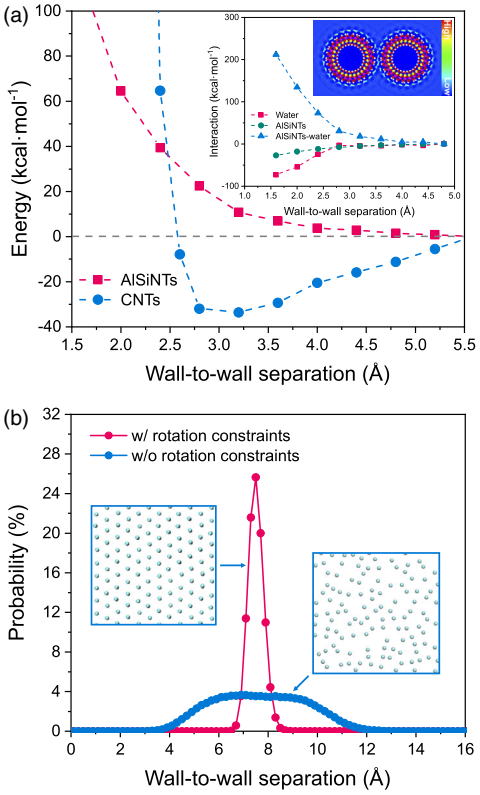

FIG. 4. (a) Relative energies between two AlSiNTs or CNTs suspended in water vs the wall-to-wall distance, computed by all-atom simulations. The inset shows decomposed contributions of water-water, AlSiNTs-AlSiNTs, and AlSiNTs-water for the AlSiNT system and the water density map surrounding nanotubes at a separation of 3.2 Å. (b) Distribution of the shortest intertubular distance between AlSiNTs with or without rotational constraints (3D vs 2D simulations). The insets show the corresponding configuration snapshots. Both systems have an average wall-to-wall distance of 7.5 Å.

To simulate the colloid systems of nanotubes, CG models are developed (see methods and Fig. S7 in the Supplemental Material [14]). The simulated system evolution of AlSiNTs and CNTs, starting from rather isotropic configurations, can be seen in Fig. S7c [14]. Because of the solvation-induced repulsion between AlSiNTs, it imposes rotational constraints on AlSiNTs and subsequently leads to highly ordered hexagonal arrays [inset of Fig. 4(b)] to minimize energetically unfavorable overlaps. To confirm the role of the constrained rotation, we further perform 2D simulations where the rotational motion is disabled. Without the rotational constraints, Fig. 4(b) shows that the distribution of the intertubular distance becomes significantly wider and an ordered structure indeed cannot be achieved. For CNTs featuring attractive intertubular forces, nanotubes aggregate (Supplemental Material, Fig. S7c [14]).

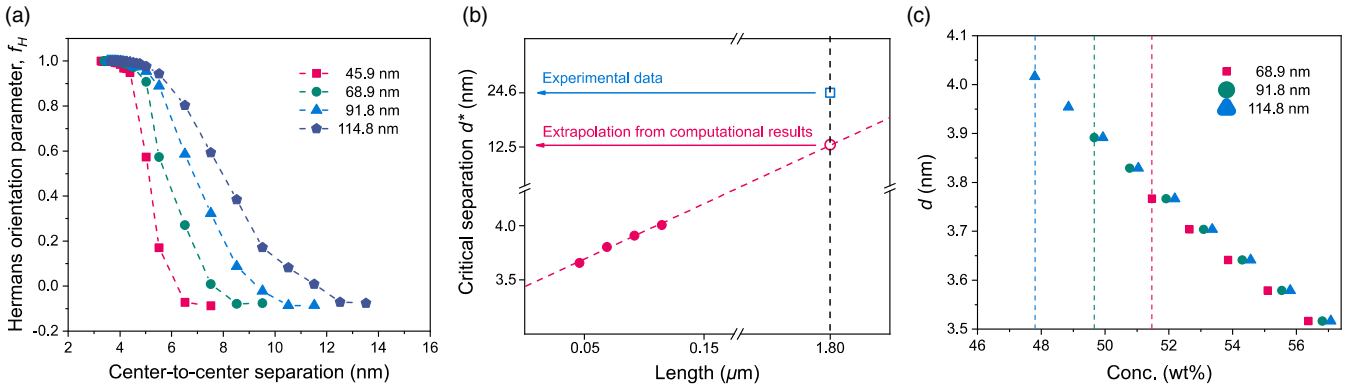

FIG. 5. Phase transition of AlSiNTs. (a) f_H vs average separation distance for different tube lengths (the z direction of the simulation box is used as the reference axis). (b) Relationship between the critical separation distance (d^*) and the nanotube length. For simplicity, a threshold of $f_H = 0.9999$ is used to determine if hexagonal arrays are formed. A fitted (dashed) line is also given. The figure also shows the extrapolated critical separation distance for 1.8 μm AlSiNTs and that observed from SAXS. (c) Intertubular distance vs concentrations observed in simulations for nanotubes with varying lengths. The dashed line indicates the critical concentration (or separation) to form colloidal crystals for each studied tube length.

The f_H of AlSiNTs vs separation distance is also computed for tubes with varying lengths [Fig. 5(a)]. The separation distance, inversely proportional to the AlSiNT concentration, is defined as the average spacing between nanotubes when tubes are perfectly aligned and dispersed. Consistent with SAXS and cryo-TEM, the results show an s-shaped curve with a transition from highly aligned structures (i.e., $f_H = \sim 1$) to randomly orientated configurations (i.e., $f_H = \sim 0$) upon decreasing the concentration. The slightly negative f_H determined for the disorder phase is an artifact resulting from the simulation domain with a smaller average intertubular spacing along the z direction relative to that along the x–y plane (see methods in the Supplemental Material [14]). The relationship between the critical separation (or concentration) to achieve hexagonal arrays and the nanotube length is also quantified; as summarized in Fig. 5(b), the critical distance increases linearly with the tube length. This appears reasonable as the imposed rotational constraints on longer nanotubes are more pronounced. Based on this, the critical distance for 1.8 μm AlSiNTs is predicted to be 12.5 nm. Considering the uncertainties involving in both the AA and CG calculations, such as the assumption of rigid structures, the force field parameters adopted, and the z spacing used to setup the CG calculations, a factor of 2 deviation as compared to the SAXS results (i.e., 24.6 nm) can be deemed as a good agreement. Our simulations also predict a monotonic decrease of the separation distance as a function of concentration [Fig. 5(c)]. We note that, although these simulated systems have notably shorter tube lengths (or larger concentrations) relative to experimental ones due to the consideration of computational costs, the results from studying nanotubes of varying lengths have quantitatively informed the behavior of nanotube alignment as a function of tube length and concentration.

Conclusions.—This study reports that constraining the rotational motion of low-dimensional nano-objects by utilizing the intrinsic solvation-induced repulsive forces can achieve a spontaneously well-aligned colloidal superstructure with controllable separation distances in dilute and spacer-free solutions. Highly ordered hexagonal arrays of AlSiNTs suspended in water form with a separation distance of more than 20 nm. The superalignment is quantitatively probed *via* bulk (SAXS) and local (cryo-TEM) characterization techniques, with atomistic understandings gained from MD simulations. Our findings should be generalizable for other nanotube species with good solvation and a uniform length distribution. For systems fulfilling these two criteria, the desirable separation distance may be precisely controlled by varying the tube length and/or the tube concentration. The outcomes of this study can facilitate the future development of well-aligned colloidal systems in dilute solution for applications such as visible-UV photonics [34] and nanolithography [35].

This work was supported from the Young Scholar Fellowship Program by Ministry of Science and Technology (MOST) in Taiwan, under Grant No. MOST 108-2636-E-002-015. The authors acknowledge the computational resources from the Ohio Supercomputer Center. The authors also thank An-Chih Yang and Ting-Yu Wang for their assistance on the cryo-TEM imaging for the early-stage discovery of AlSiNT superalignment. C. Y. S. and C. C. H. thank the MOST in Taiwan for the grant (No. MOST106-2221-E-194-055) as well as the NSRRC in Taiwan for the beamtimes.

*These authors contributed equally.
†Corresponding author.
dunyen@ntu.edu.tw
‡Corresponding author.
chmcch@ccu.edu.tw
§Corresponding author.
lin.2645@osu.edu

[1] X. Ye *et al.*, Nat. Chem. **5**, 466 (2013).

[2] J. Henzie, M. Grünwald, A. Widmer-Cooper, P. L. Geissler, and P. Yang, Nat. Mater. **11**, 131 (2012).
[3] B. Li, F. Wang, D. Zhou, Y. Peng, R. Ni, and Y. Han, Nature (London) **531**, 485 (2016).
[4] H. Mundoor, B. Senyuk, and I. I. Smalyukh, Science **352**, 69 (2016).
[5] G. Distefano, H. Suzuki, M. Tsujimoto, S. Isoda, S. Bracco, A. Comotti, P. Sozzani, T. Uemura, and S. Kitagawa, Nat. Chem. **5**, 335 (2013).
[6] B.-G. Kim, E. J. Jeong, J. W. Chung, S. Seo, B. Koo, and J. Kim, Nat. Mater. **12**, 659 (2013).
[7] I. Tomiki, M. Jun-ichi, and Y. Yanlei, Angew. Chem., Int. Ed. Engl. **46**, 506 (2007).
[8] E. Auyeung, J. I. Cutler, R. J. Macfarlane, M. R. Jones, J. Wu, G. Liu, K. Zhang, K. D. Osberg, and C. A. Mirkin, Nat. Nanotechnol. **7**, 24 (2012).
[9] M. N. O'Brien, M. R. Jones, B. Lee, and C. A. Mirkin, Nat. Mater. **14**, 833 (2015).
[10] M. Siavashpouri, C. H. Wachauf, M. J. Zakhary, F. Praetorius, H. Dietz, and Z. Dogic, Nat. Mater. **16**, 849 (2017).
[11] M. Hu, L. Qian, R. P. Briñas, E. S. Lymar, and J. F. Hainfeld, Angew. Chem. **119**, 5203 (2007).
[12] B. Li, D. Zhou, and Y. Han, Nat. Rev. Mater. **1**, 15011 (2016).
[13] E. Paineau, M.-E. M. Krapf, M.-S. Amara, N. V. Matskova, I. Dozov, S. Rouzière, A. Thill, P. Launois, and P. Davidson, Nat. Commun. **7**, 10271 (2016).
[14] See Supplemental Material at http://link.aps.org/supplemental/10.1103/PhysRevLett.123.238002 for synthesis of aluminosilicate nanotubes (AlSiNTs), materials characterizations, computational methods, and supplemental figures and tables.
[15] L. A. Feigin and D. I. Svergun, *Structure Analysis by Small-Angle X-Ray and Neutron Scattering* (Plenum Press, New York, 1987).
[16] B. Angelov, A. Angelova, R. Mutafchieva, S. Lesieur, U. Vainio, V. M. Garamus, G. V. Jensen, and J. S. Pedersen, Phys. Chem. Chem. Phys. **13**, 3073 (2011).
[17] A. Sundblom, C. L. P. Oliveira, A. E. C. Palmqvist, and J. S. Pedersen, J. Phys. Chem. C **113**, 7706 (2009).
[18] B. K. Vainshtein, *Diffraction of X-rays by Chain Molecules* (Elsevier, Amsterdam, 1966).
[19] R. H. Guo, C. H. Hsu, C. C. Hua, and S. A. Chen, J. Phys. Chem. B **119**, 3320 (2015).
[20] Y. H. Wen, P. C. Lin, C. C. Hua, and S. A. Chen, J. Phys. Chem. B **115**, 14369 (2011).
[21] H. L. Yi, C. H. Wu, C. I. Wang, and C. C. Hua, Macromolecules **50**, 5498 (2017).
[22] E. Grelet and R. Rana, Soft Matter **12**, 4621 (2016).
[23] P. Levitz, M. Zinsmeister, P. Davidson, D. Constantin, and O. Poncelet, Phys. Rev. E **78**, 030102(R) (2008).
[24] T. Loerting, C. Salzmann, I. Kohl, E. Mayer, and A. Hallbrucker, Phys. Chem. Chem. Phys. **3**, 5355 (2001).
[25] G. I. Yucelen, D. Y. Kang, I. Schmidt-Krey, H. W. Beckham, and S. Nair, Chem. Eng. Sci. **90**, 200 (2013).
[26] S. Mukherjee, V. A. Bartlow, and S. Nair, Chem. Mater. **17**, 4900 (2005).
[27] M. Almgren, K. Edwards, and G. Karlsson, Colloids Surf. A **174**, 3 (2000).
[28] H. Su, P. Bomans, H. Friedrich, and N. Sommerdijk, in *European Microscopy Congress 2016: Proceedings* (Wiley-VCH Verlag GmbH & Co. KGaA, Weinheim, 2016).
[29] S. Plimpton, J. Comput. Phys. **117**, 1 (1995).
[30] K.-H. Liou, D.-Y. Kang, and L.-C. Lin, ChemPhysChem **18**, 179 (2017).
[31] P. Mark and L. Nilsson, J. Phys. Chem. A **105**, 9954 (2001).
[32] R. T. Cygan, J.-J. Liang, and A. G. Kalinichev, J. Phys. Chem. B **108**, 1255 (2004).
[33] T. Werder, J. H. Walther, R. L. Jaffe, T. Halicioglu, and P. Koumoutsakos, J. Phys. Chem. B **107**, 1345 (2003).
[34] E. Lidorikis and A. C. Ferrari, ACS Nano **3**, 1238 (2009).
[35] J. Bai, X. Duan, and Y. Huang, Nano Lett. **9**, 2083 (2009).